Supplement of Geosci. Model Dev., 19, 6121–6142, 2026
https://doi.org/10.5194/gmd-19-6121-2026-supplement

Geoscientific Model Development
Open Access
EGU

Supplement of

Cleo: the numerical methods of a new superdroplet model including a droplet breakup algorithm (v0.52.0)

Clara J. A. Bayley et al.

Correspondence to: Clara J. A. Bayley (clara.bayley@mpimet.mpg.de)

S1 Box-Model Verification of Collisions with a Fixed Coalescence Efficiency and a Fixed Number of Fragments

Figure S1 shows the same setup as for the test of SDM collisions as in Shima et al. (2009, Sec. 5.1.4, Figure 2), which is also used to produce Figure 9 in Section 6.2 of the main manuscript. However, here we show the mass density distribution after $120\,\mathrm{s}$ for simulations comparable to de Jong et al. (2023, Sec. 4.1.1, Fig. 7a). Specifically, the simulations use 8192 superdroplets and the hydrodynamic collision kernel with collision efficiencies from Long (1974). Collisions either result in only coalescence (as per the original treatment of collisions; Shima et al., 2009), or use our extended treatment. In the extended treatment for these simulations rebound is excluded and a random number is compared to a fixed coalescence efficiency, $E_\mathrm{c} = 0.95$, to determine if breakup or coalescence occurs. The number of fragments produced in the event of breakup is also fixed such that $N_\mathrm{frag} = 4.0$, 16.0 or 64.0.

The results are qualitatively the same as de Jong et al. (2023) but the droplets are generally larger for the same fixed number of fragments. As the number of fragments increases, the mean droplet size decreases and the distribution broadens. As explained by de Jong et al. (2023), this broadening of the size distribution is generally expected because the small droplets produced by collisional breakup have a wide range of collision rates. For the same N_frag, the mean of the distribution is, however, noticeably larger than de Jong et al. (2023), possibly because we do not allow for multiple collisional breakup events in a single time-step and therefore our algorithm produces fewer fragments with larger sizes for cases in which PySDM instead iteratively produces N_frag fragments.

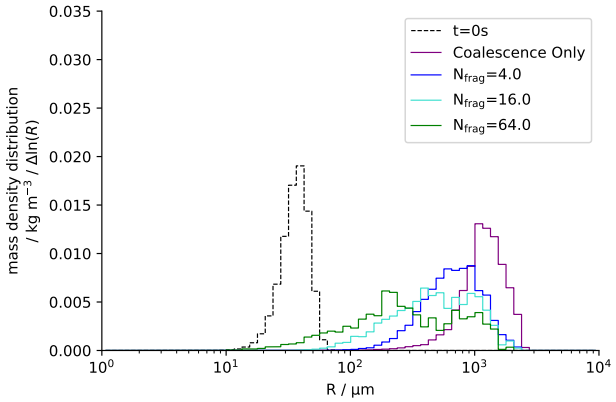

Figure S1. Test of SDM collisions after 120 s as in Shima et al. (2009, Sec. 5.1.4, Figure 2) but including idealised breakup scenarios. The colour indicates the collision outcome, either in which only coalescence can occur, or in which a fixed number of fragments is produced if breakup occurs. For the simulations involving breakup, the coalescence efficiency is fixed, $E_c = 0.95$. Additionally the initial condition of all the simulations is shown (black dashed line). This figure is comparable to de Jong et al. (2023, Sec. 4.1.1, Fig. 7a).

S2 Droplet Motion Verification with Fall Speeds

Figure S2 shows the same plot as Figure 11 in Section 6.3 of the main manuscript except that we run the simulation for 2 hours and include the terminal velocity of the tracers according to Rogers et al. (1993). We also model condensation/evaporation with a 1 s time-step to make the tracers grow enough to have an appreciable fall speed but not so large that they fall out of the domain. The thermodynamics are time-invariant throughout the simulations, with pressure and temperature following hydrostatic profiles with surface values of 1013.15 hPa and 289 K respectively, and the domain is fully supersaturated throughout (supersaturation = 1.0).

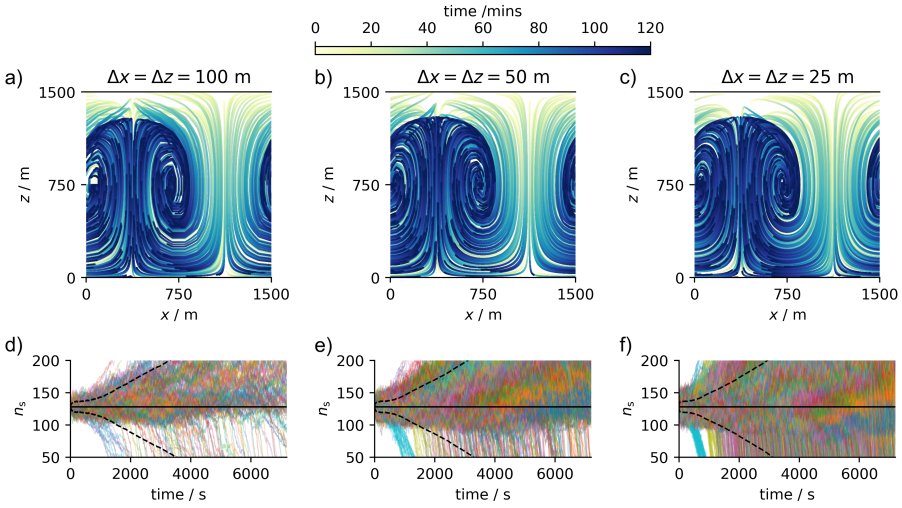

Figure S2. Results of tracer particle motion with fall speeds in the 2-D divergence free laminar flow described by Arabas et al. (2015). Grid-spacing decreases in each column from left to right. Panels a, b, and c show the trajectories of a random sample of 500 superdroplets; Panels d, e, and f show the number of superdroplets in each grid-box over time, as well as the mean across all the grid-boxes (black; solid) and the standard deviation (black; dashed). The variance is caused by superdroplets leaving/entering different grid-boxes. The fall speeds create an asymmetry in the particle trajectories such that they cluster in the convergence zones of the domain.

References

Arabas, S., Jaruga, A., Pawlowska, H., and Grabowski, W. W.: libcloudph++ 1.0: a single-moment bulk, double-moment bulk, and particle-based warm-rain microphysics library in C++, Geoscientific Model Development, 8, 1677–1707, https://doi.org/10.5194/gmd-8-1677-2015, 2015.

de Jong, E., Mackay, J. B., Bulenok, O., Jaruga, A., and Arabas, S.: Breakups are complicated: an efficient representation of collisional breakup in the superdroplet method, Geoscientific Model Development, 16, 4193–4211, https://doi.org/10.5194/gmd-16-4193-2023, 2023.

Long, A. B.: Solutions to the Droplet Collection Equation for Polynomial Kernels, Journal of Atmospheric Sciences, 31, 1040 – 1052, https://doi.org/10.1175/1520-0469(1974)031<1040:STTDCE>2.0.CO;2, 1974.

Rogers, R. R., Baumgardner, D., Ethier, S. A., Carter, D. A., and Ecklund, W. L.: Comparison of Raindrop Size Distributions Measured by Radar Wind Profiler and by Airplane, Journal of Applied Meteorology and Climatology, 32, 694 – 699, https://doi.org/10.1175/1520-0450(1993)032<0694:CORSDM>2.0.CO;2, 1993.

Shima, S., Kusano, K., Kawano, A., Sugiyama, T., and Kawahara, S.: The super-droplet method for the numerical simulation of clouds and precipitation: a particle-based and probabilistic microphysics model coupled with a non-hydrostatic model, Quarterly Journal of the Royal Meteorological Society, 135, 1307–1320, https://doi.org/10.1002/qj.441, 2009.